Hindawi
Advances in Materials Science and Engineering
Volume 2018, Article ID 8025708, 12 pages
https://doi.org/10.1155/2018/8025708

Research Article

Experimental Study of Pulsed Discharge Underwater Shock-Related Properties in Pressurized Liquid Water

D. C. Bian, D. Yan, J. C. Zhao, and S. Q. Niu

College of Mining Engineering, Taiyuan University of Technology, Taiyuan 030024, China

Correspondence should be addressed to J. C. Zhao; zhaojinchang@tyut.edu.cn

Received 25 April 2017; Accepted 1 November 2017; Published 23 January 2018

Academic Editor: Renal Backov

Engineering background of hydraulic fracturing is applied to improve the permeability of unconventional gas wells, such as coal seams and shale gas wells, by a pulsed discharge mechanism. We studied the general relations between water shock wave properties (the maximum pressure, wave velocity, and energy conversion efficiency), the discharge voltage, and hydrostatic pressure during high-voltage pulsed discharge experiments in pressurized liquid water. The following observations were made: (1) when the discharge voltage increased from 7 kV to 13 kV, the maximum pressure increased from 12.6 MPa (hydrostatic pressure $P_H = 12$ MPa) to 40 MPa ($P_H = 6$ MPa), wave velocity increased from 1418 m/s ($P_H = 12$ MPa) to 1454 m/s ($P_H = 6$ MPa), and energy conversion efficiency increased from 9% to 11%, and (2) when hydrostatic pressure increased from 0 MPa to 12 MPa, the maximum pressure and wave velocity augmented and then diminished slowly (the critical hydrostatic pressure occurs in the 3 to 6 MPa range), whereas the change of energy conversion efficiency was not obvious. Their properties are explained by the variation of electrical parameters during the pulsed discharge.

1. Introduction

The most direct and effective method to improve oil and gas production is reservoir fracturing, which can substantially improve reservoir permeability [1, 2]. Because of significant variations in the characteristics of these unconventional gas reservoirs (e.g., coal gas and shale gas) [3, 4], the traditional fracturing techniques are not efficient to improve reservoir permeability. Problems such as low efficiency, poor degree of control, damage caused by the fracturing fluid to the reservoir and underground environment, and large water consumption are very common [5, 6]. Therefore, the natural gas mining industry urgently needs a better fracturing technology for these unconventional types of extraction.

The phenomenon of high-voltage pulsed discharge in water (HVPD) has been applied to several domains, such as mechanical processing, lithotripsy, and waste water treatment [7–9]. In recent years, there has been some investigation into the application of HVPD to remove oil and gas well plugs and for reservoir fracturing improvements [6, 10]. The water shock waves (WSWs) produced by HVPD are the main power source behind the fracturing of gas reservoirs, the coal and rocks of the gas reservoirs will exhibit different fracturing characteristics under different WSWs. [11]. Thus, any research of this technology must consider the properties of WSW. Considering the depth of oil and gas wells may range from hundreds to thousands of meters, it is important to consider the effect of hydrostatic pressure (P_H) on plasma breakdown, WSW excitation, and transfer processes.

There are many researchers investigating the characteristics of WSWs produced by HVPD [12–19], but few of them considered the effects of P_H on WSWs. Furthermore, other researchers carried out some experiments to study the electrical characteristics of pulsed discharge in pressurized water [20–22]. The results showed that P_H increased the breakdown voltage of water dielectric and hindered the processes of HVPD and the formation of plasma channels. Schaefer's results showed that the larger the P_H, the smaller the bubble maximum radius and the higher the peak frequency [23]. Jeffrey conducted a theoretical study revealing that the bubble period and the minimum rarefaction

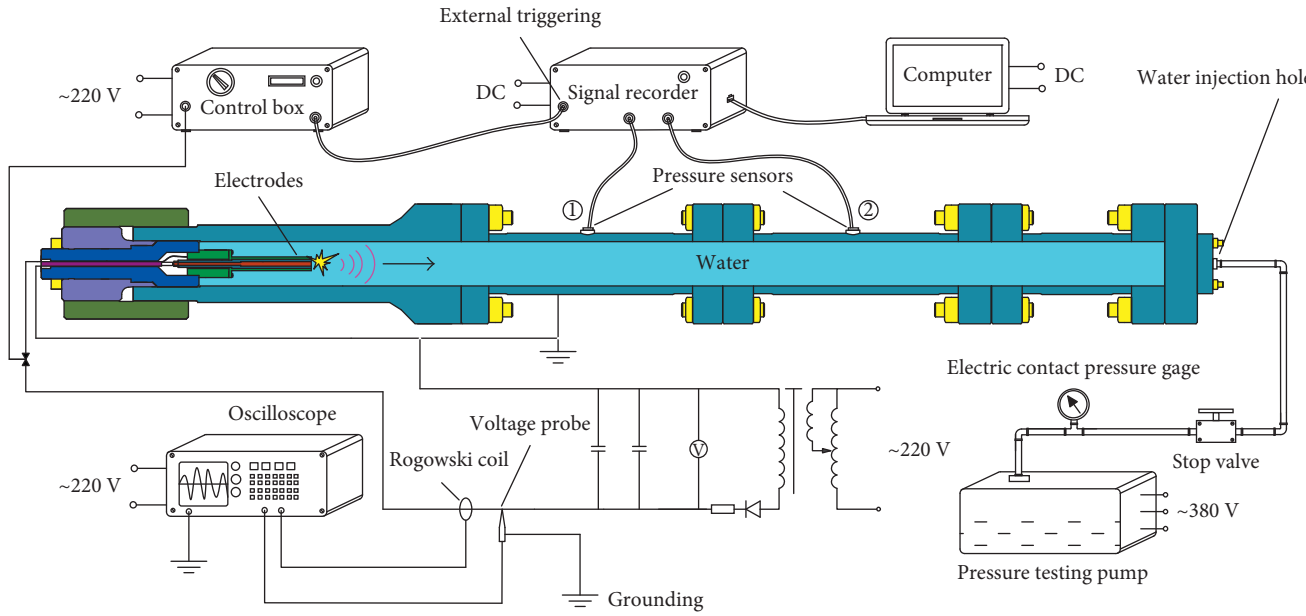

Figure 1: Schematic diagram of the experimental instruments.

pressure were dependent on P_H, while the first peak pressures of WSW were unrelated to P_H when $P_H < 0.9$ MPa [24]. Based on Jeffrey's results, Lu presented a new model including bound-bound transitions in the calculation of the thermal radiation power [25]. His calculations agreed with the experimental results of Jeffrey. However, researchers determined the influence of law of P_H on WSWs through theoretical study of the HVPD in pressurized liquid water. Moreover, comparison with experimental results was restricted to $P_H < 0.9$ MPa. Therefore, it is unclear if the first maximum pressure of the WSW is unrelated to P_H values > 0.9 MPa [23]. Investigating the relation between the pulsed discharge voltage U_D, hydrostatic pressure P_H, and water shock wave properties (e.g., the maximum pressure P_M, wave velocity D_W, and energy conversion efficiency η) is important to better understand the phenomenon of HVPD and characterize the impact load of WSWs. This can lead to improvements in the construction technologies for reservoir fracturing.

This study establishes the functional relations between P_M, D_W, and η and U_D and P_H during HVPD experiments. The characteristics of WSW were then controlled by adjusting U_D and P_H. Finally, we generated controlled and repeatable optimized shock loads that conformed to the requirements of fracturing rock mass.

2. Experimental Instruments and Design

2.1. Principles of Experiments. Our studies were based on the fundamental principle of the electrohydraulic effect. A conventional 220 V single-phase alternating current will charge the pulsed energy storage capacitor bank after filtering, boosting, and rectifying by corresponding circuits. The capacitance of the capacitor bank was fixed, and the stored energy was controlled by U_D. During the HVPD experiments, a trigger signal was generated by the control system to close the discharge switch. The energy stored in the capacitor bank was loaded instantaneously into the water body located between the discharge electrodes. A high-energy density plasma channel was generated and expanded rapidly from the inside to the outside. The excited pulse was transmitted through water in a given direction forming a shock wave. The relations between U_D, P_H, and water shock wave properties were investigated by monitoring and analyzing the voltage, current, and WSW waveforms.

2.2. Structure of the Experimental Instruments. The experimental equipment was composed of a HVPD system, a pressure-bearing pipeline system, and a measuring system (Figure 1).

The capacitance of the capacitor bank in the pulsed discharge cabinet was set at $C = 60\,\mu$F, and its rated operational voltage was 15 kV. The discharge voltage of two MFM30-15 pulse capacitors was continuously adjusted within the prescribed range. A coaxial copper configuration was set in the electrode to make the WSW propagate along the pipeline horizontal direction and avoid electrode high-voltage ablation. This set up ensures the stability of the HVPD and meets the strength of the electrode. The electrode was 300 mm long, and the high- and low-voltage electrode spacing (l) was 5 mm. The discharge chamber presents a tubular structure (Figure 2). The axle sleeve and electrode structure were sealed and fixed at one end of the discharge chamber by a threaded sleeve and clamping cap. The flange plate was located at the other end of the discharge chamber, which was connected to the pressure-bearing pipeline of the WSW. Figure 3 illustrates the pressure-bearing pipeline system. It contains two long pipes (1 m in length) and one short pipe (0.5 m length) connected by flange plates. The initial P_H in the pipeline

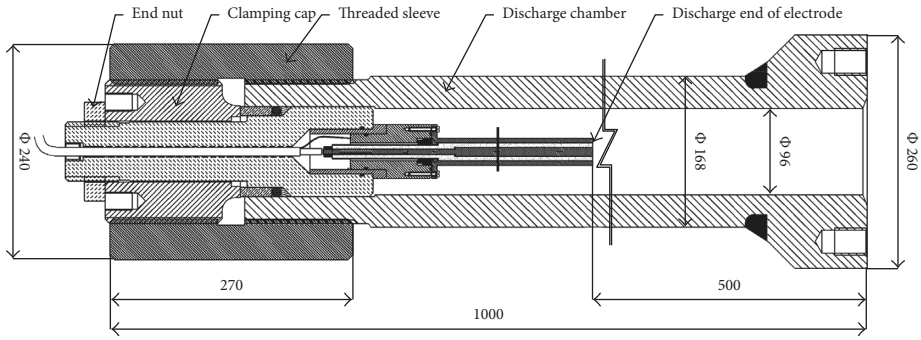

Figure 2: Schematic diagram of the discharge chamber structure.

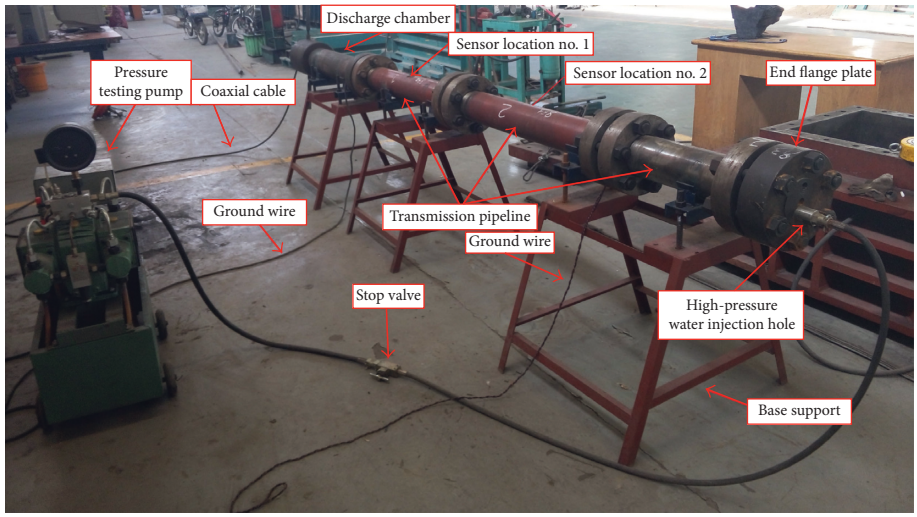

Figure 3: Photograph of the pressure-bearing pipeline system.

system was supplied by a BD-4DSB-16 pressure testing pump producing a maximum pressure of 16 MPa. Two pressure sensors, numbered 1 and 2, were installed on the pipeline wall. The CY400 high-frequency dynamic piezoresistive pressure sensor was selected for data acquisition. The sensor provided a range between 0 and 50 MPa with a 150% overload capacity. The maximum sampling frequency was 1 MHz. The bandwidth and response time of the pressure sensor are 1/(400 kHz) and 0.3 μs, respectively. The signals collected by the sensors were amplified and processed using a TST6250 instantaneous signal recorder. The measured precision was 0.01 MPa for dynamic pressure and 0.1 m/s for velocity.

The external trigger interface of the instantaneous signal recorder was connected to a discharge control box. The current signal was monitored by a self-integrating Rogowski coil with a sensitivity of 38 kA/mV. The voltage signal was detected using a Tektronix P6015A high-voltage probe. The current and voltage signals were loaded into an Agilent DSO6014A digital oscilloscope.

2.3. Anti-Interference Measures of the Experimental Instruments. A significant energy conversion resulted from the breakdown of the water gap by HVPD. This was accompanied by strong electromagnetic radiations and a voltage/current break in the loop of the instruments [26]. We thus applied the following anti-interference measures:

(1) Power supply: a single-phase alternating current (220 V, 50 Hz) was supplied to the HVPD system. Internal direct current rechargeable batteries were used for the measuring system, that is, the signal recorder and computer, which was sensitive to interference signals. Therefore, a conduction coupling interference formed by the power supply was avoided.

(2) Grounding measures: the pressure-bearing pipeline was connected firmly to the pulsed capacitor grounding point, and the measuring system is insulated at this grounding point. The charge–discharge control box, digital oscilloscope, and high-voltage probe must be grounded separately. Floating was used in the case of the signal recorder [27].

(3) Electromagnetic shielding measures: we used piezoresistive pressure sensors with metal shielding providing a clear and strong resistance to interference. We also selected an instantaneous signal recorder with a complete metal shell. The instantaneous signal

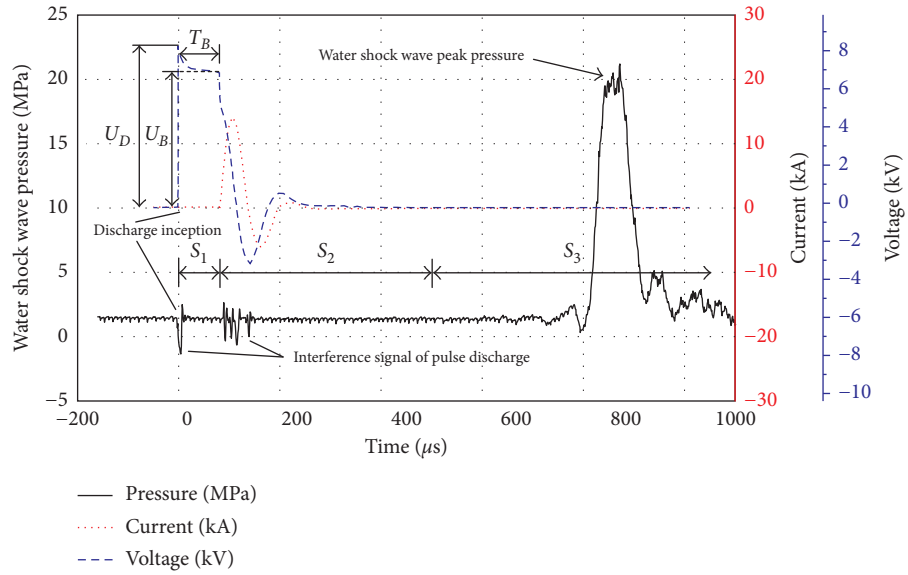

Figure 4: Diagram of the voltage, current, and pressure waveforms versus time for a typical HVPD process (P_H: 1 MPa; U_D: 7000 V).

recorder and the Rogowski coil were placed in an aluminum shielding box.

(4) Wires: we kept the wires in the experiment as short as possible. The two wires located between the capacitor and the electrode are coaxial cables. Radiation coupling and electrical loop inductance were reduced as much as possible.

2.4. Experimental Process. U_D values of 7, 9, 11, and 13 kV were used, respectively. P_H was increased in 1 MPa steps in the 0 to 4 MPa range and in 2 MPa steps in the 4 to 12 MPa range. The distance between No. 1 sensor and the electrode, and between Nos. 1 and 2 sensors, is 1 m. Several tests were repeated for each U_D and P_H to eliminate random system errors [20, 28]. Water in the pipeline was replaced before each test to ensure constant temperature ($T = 20^{\circ}$C) and conductivity ($\rho = 340\,\mu$S/cm) [29, 30]. The voltage, current, and WSW pressure waveforms were monitored by the measuring system. Note that the shock wave peak pressure measured by the sensor included P_H. In the following discussion, P_M does not include P_H.

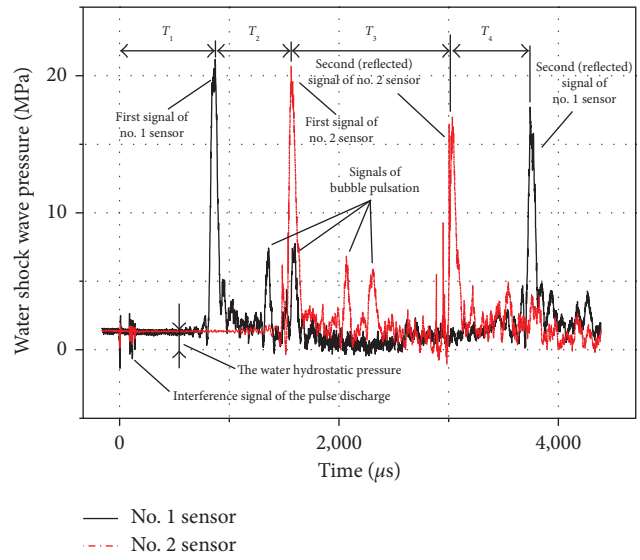

Figure 5: Typical WSW waveforms obtained by two pressure sensors (P_H: 1 MPa; U_D: 7000 V).

3. Analysis of Experimental Data

The voltage, current, and WSW pressure waveforms from a typical HVPD process are illustrated in Figure 4. The transfer process of the WSW in the pipeline is monitored by two pressure sensors on the pipeline wall. Typical pressure waveforms are illustrated in Figure 5.

WSWs are generated after the discharge gap breakdown of the electrode and propagated from the end of the electrode to the bottom of the pipeline. The pressure was measured by the No. 1 sensor (Time-consuming T_1). After transmission on 1 m, the signal was captured by No. 2 sensor (Time-consuming T_2). The WSW is propagated and reaches the bottom of the pipeline after transmission on 1 m. Then, it is reflected by the end flange and successively propagated to No. 2 (Time-consuming T_3) and No. 1 sensor (Time-consuming T_4).

3.1. Relationship between U_D and WSW Properties. The voltage and current waveforms were analyzed to determine the values of breakdown voltage U_B, discharge breakdown time delay T_B, loop resistance R_L, peak current I_P (the first half-wave), and peak power P_P [31].

The plots reveal T_B gradually decreasing with increasing U_D values when P_H remained constant (Figure 6). Theoretically, increasing the U_D values will enhance the field strength difference between the two ends of the gap,

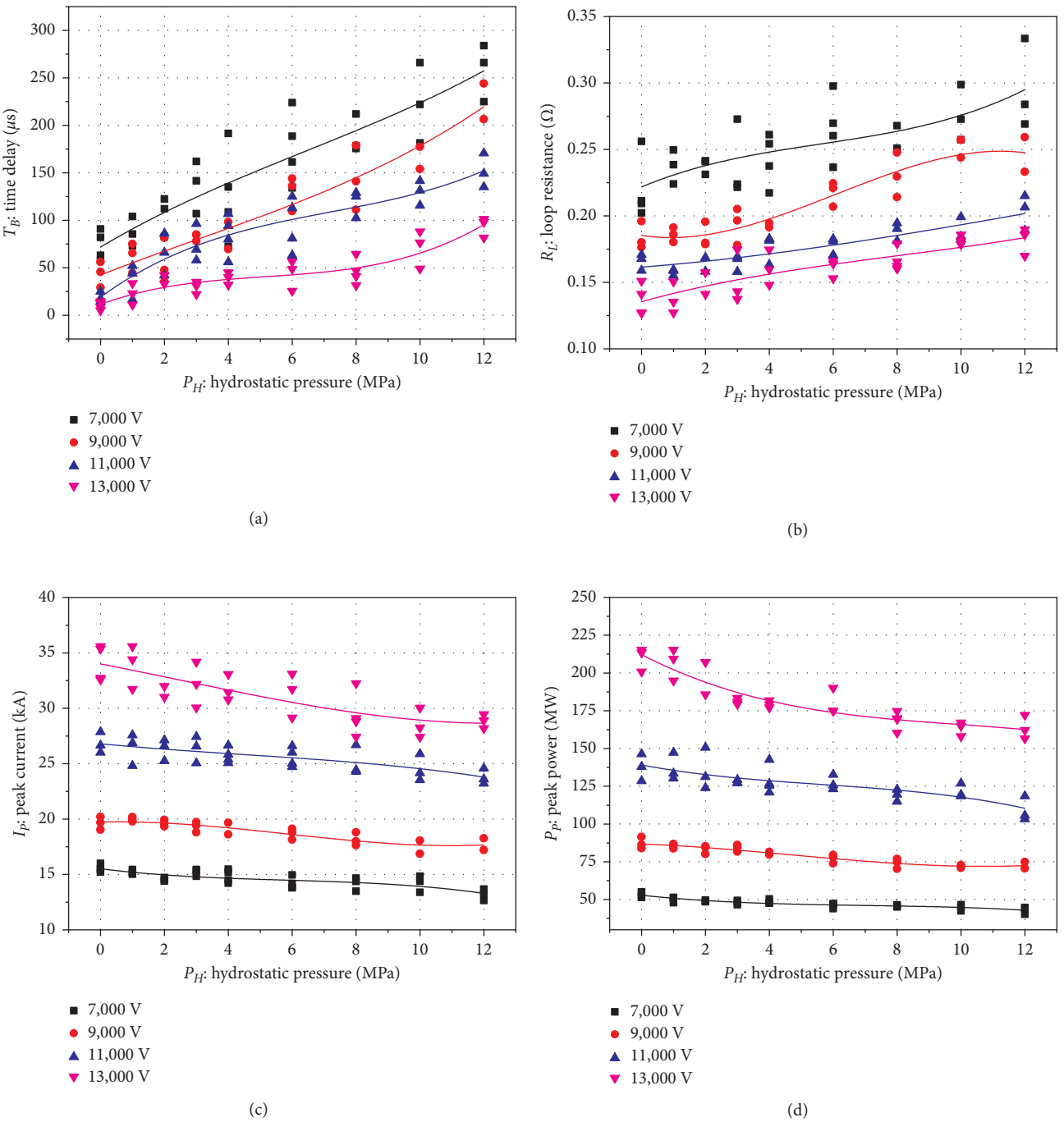

Figure 6: Variation diagram of (a)T_B, (b) R_L, (c) I_P, and (d) P_P versus P_H for a range of U_D and P_H values.

accelerating the water ionization and gasification velocity [32]. Then, an ionization avalanche is started, increasing the growth speed of the main plasma channel and decreasing the T_B values during the discharge process. The energy input into the plasma channel after the breakdown was enhanced by increasing the U_D values. As a result, the plasma temperature grew, inducing a higher ionization rate and conductivity. The channel pressure also augmented due to the higher plasma temperature, accelerating the expansion of the channel, enhancing the conductive cross section, and finally leading to a decrease in channel resistance [33]. The plasma is the energy-transforming component of the HVPD. Augmenting the U_D values reduced the resistance of the plasma, which increased the I_P and P_P values in the plasma channel.

P_M and D_W increased with increasing U_D when the P_H values were fixed. This is explained by the empirical equation of the water shock wave peak pressure (P_M) [34]:

$$P_M = k(Q_B)^{\alpha}, \tag{1}$$

where k is a constant related to the experimental environment, Q_B is the breakdown energy, and α forms the

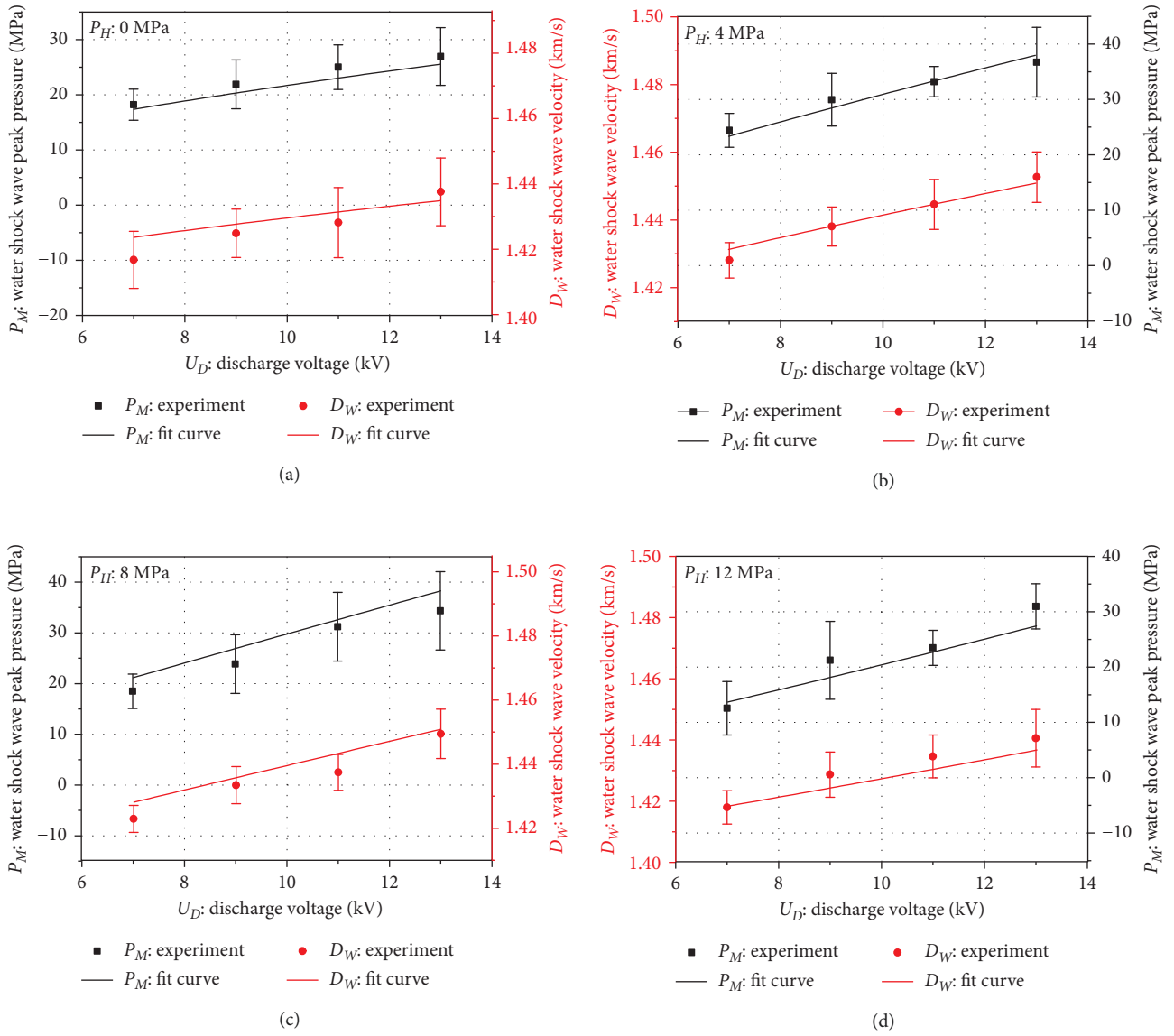

Figure 7: Variations between U_D, P_M, and velocity D_W under four different P_H settings: (a) 0 MPa, (b) 4 MPa, (c) 8 MPa, and (d) 12 MPa.

attenuation coefficient of the water shock wave associated with the electrode structure.

Therefore, the P_M value is enhanced by increasing the U_D value when all other parameters are constant. For a weak water shock wave ($P_M < 0.1$ GPa), the transfer process is isentropic, producing the following relation between wave velocity (D_W) and P_M [35] such as

$$D_W = c_0\left(1 + \frac{n+1}{2n}\frac{P_M}{B}\right)^{1/2} \cong c_0\left(1 + \frac{n+1}{4n}\frac{P_M}{B}\right), \quad (2)$$

where c_0 is the sound velocity of water before perturbation, $n = 7.15$, and $B = 299$ MPa.

Figure 7 indicates similar increasing trends of D_W and P_M values with the augmentation in U_D.

The experience formula for computing the energy of WSW is as follows [36, 37]:

$$E_s = \frac{S}{\rho v}\int_0^{+\infty} P^2 dt, \quad (3)$$

where E_S is the energy of WSW in J, S is the wavefront area in m^2, ρ is the density of water in kg/m^3, v is the velocity of WSW in m/s, and P is the pressure of WSW in Pa.

The ratio between the WSW energy (E_S) to the electrical energy stored in the capacitors (E) is defined as the energy conversion efficiency (η):

$$\eta = \frac{E_S}{E} \times 100\% = \frac{2S}{\rho v C U_D^2}\int_0^{+\infty} P^2 dt \times 100\%. \quad (4)$$

From Figure 8, we observed a η value is roughly around 10% increasing slightly with the U_D value when the P_H values were fixed. This is principally related to the increase in U_D that reduces T_B and then lowers the leakage loss of energy and improves the energy conversion efficiency.

3.2. Relation between P_H and WSW Properties. We cannot ignore P_H when applying HVPD during unconventional gas well fracturing and in deep sea environments. Kao [38] and Korobeinikov [39] developed a bubble initiation theory to explain the plasma breakdown process, in which the environmental pressure significantly affected the breakdown field strength of a liquid. The influence of P_H was determined by HVPD experiments in pressurized liquid water. During the pulsed discharge process, P_H shows "inhibiting" and "enhancing" effects. The inhibiting effect is caused by the compression and hindering of the plasma channel expansion shock, since P_H lowers the initial P_M and D_W. The enhancement is generated by a reduction of the attenuation coefficient during the transfer of the WSW through the water medium. When the P_H values increase, both of these effects will change P_M and D_W starting by an augmentation followed by a decrease (Figure 9). The critical hydrostatic pressure (P_{CH}) occurs in the 3 to 6 MPa range.

The inhibiting mechanism works as follows: P_H and the internal pressure within the channel and the pressure on the inner wall of the channel caused by the electric field were all applied during the channel breakdown process. The combination of these pressures causes a change in the channel radius, and P_H hinders the channel expansion [40, 41].

The experimental data (Figure 9) and theoretical models indicated that the compressive action of the external pressure on the plasma due to P_H delayed the water breakdown and caused an increase in T_B. Therefore, when the U_D value remains constant, the increase in T_B with increasing P_H values produces a lower energy input into the plasma channel. More energy is wasted as heat and infrared radiation before the plasma channel formed [42], and its electrical resistivity also increased. However, the plasma channel wall was extruded by a P_H increase. The channel expansion was lowered, leading to a conductive cross section decrease relative to a situation without P_H; this also results in a growth in electrical resistivity and I_P, whereas the channel P_P declines accordingly (Figure 6). These observations indicate that T_B and P_H increase simultaneously when U_D is constant. The maximum outward expansion pressure of the plasma also decreases.

The enhancing mechanism works as follows: The propagation of weak WSW ($p \le 100$ MPa) is isentropic. The propagation and characteristics are similar to that of sound waves in water. The research of Saul and Wagner [43] showed that the shock wave maximum pressure and velocity generated by a similar source increased with increasing water hydrostatic pressure at room temperature.

P_M and D_W augmented with increasing P_H when $0 \le P_H \le P_{CH}$. Inhibiting and enhancing effects are present during this process, but the former is limited due to a low water pressure. In this case, the enhancing effect related to P_H played a primary role.

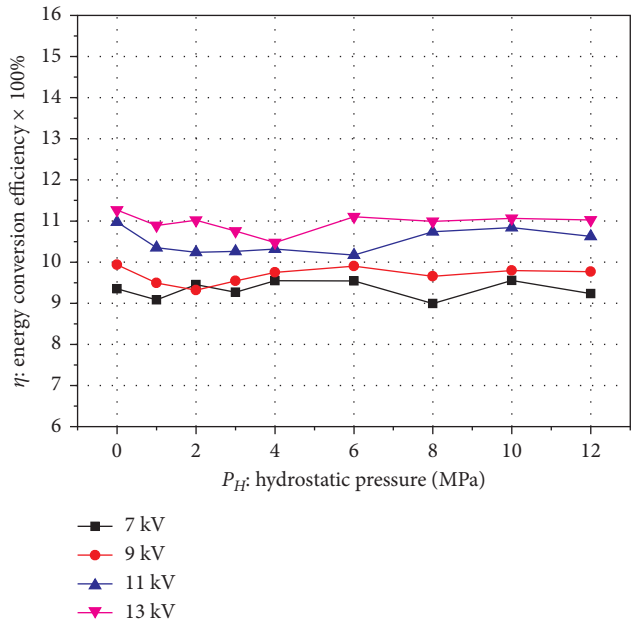

FIGURE 8: Variation diagram of η versus P_H for a range of U_D.

P_M and D_W declined slowly with increasing P_H when the inhibiting effect of P_H played a dominant role and significantly weakened P_M and D_W. Although an increased pressure also enhanced the water shock wave transfer, P_M and D_W values began to slowly diminish when $P_{CH} \le P_H$ because of the initial lowering of P_M and D_W.

Figure 8 also reveals that P_H will reduce η when pressure is applied. However, due to the increase in instability of the discharge process with increasing P_H, the change of η has no regularity.

4. Data Fitting and Contrast

Data from the literature [20, 34, 40] and experimentations reveal that T_B is a function of P_H, or $T_B = h(P_H)$. Thus, the breakdown energy Q_B is given by following equation:

$$Q_B = \frac{1}{2} C U_D^2 \exp\left(-\frac{2h(P_H)}{RC}\right), \tag{5}$$

where k and α in the empirical formula (1) are parameters related to the experimental environment and electrode geometry [44, 45]. These two parameters represent the energy conversion characteristics of the WSW in different experimental conditions [42]. We then assume k and α are related to P_H. The functions can be written as $k = f(P_H)$ and $\alpha = g(P_H)$.

Substituting (5) into (1), we produce an expression on P_M:

$$P_M = f(P_H)\left(\frac{1}{2} C U_D^2 \exp\left(-\frac{2h(P_H)}{RC}\right)\right) g(P_H). \tag{6}$$

Finally, the empirical formula (7) representing P_M in pressurized liquid water can be obtained by fitting of the

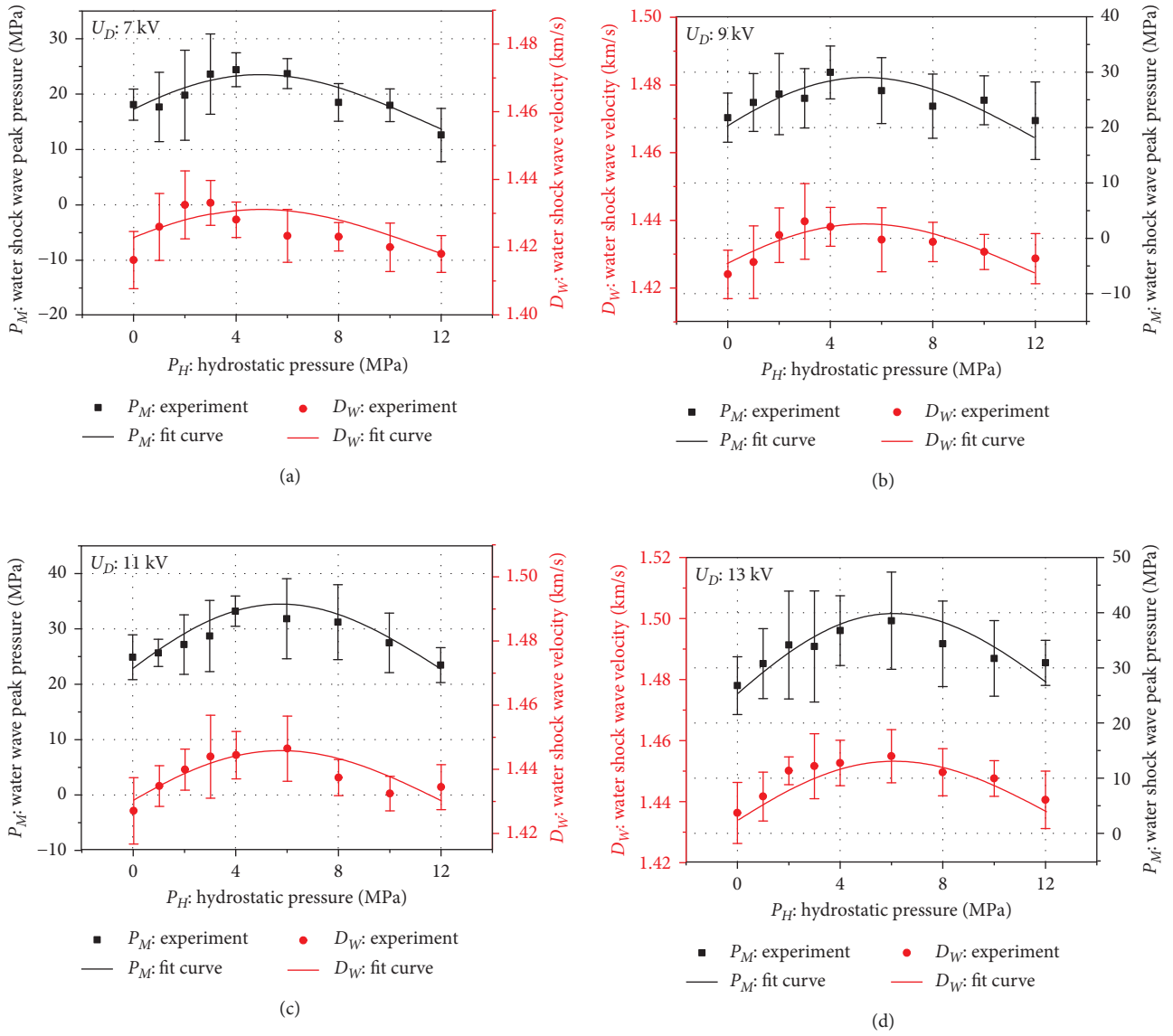

FIGURE 9: Binary diagrams showing the correlations between P_H, P_M, and D_W under four different values of U_D: (a) 7 kV, (b) 9 kV, (c) 11 kV, and (d) 13 kV.

experimental data. D_W can also be obtained by substituting (7) into (2); thus,

$$P_M = (0.7P_H + 5.59) \cdot \left(\frac{CU_D^2}{2000}\exp\left(-\frac{2}{RC}\frac{43.14P_H^2 - 5033.14}{0.41P_H + 6.14}\right)\right)^{0.02P_H+0.31}, \quad (7)$$

where P_M is the water shock wave peak pressure in MPa, P_H forms the hydrostatic pressure in MPa, U_D is the discharge voltage in kV, C defines the capacitance of the capacitor bank in μF, and R gives the equivalent resistance of the water gap in kΩ. In our experiments, $C = 60\,\mu$F and $R = 8.5\,$kΩ.

The functions $f(P_H)$ and $g(P_H)$ represent the energy conversion of the WSW in different experimental situations in (7). $f(P_H)$ and $g(P_H)$ are all linear increasing functions. This indicates that the intensity of the WSW increases with P_H, confirming the conclusions of Saul and Wagner [43] and Lu [46]. The function $h(P_H)$ represents the compression and delaying of the plasma channel expansion shock by P_H. The expression reveals that the $h(P_H)$ function increases regularly; the greater the $h(P_H)$, the more compressed the plasma channel. This is also consistent with the conclusions of Jia et al. [20], Zhang et al. [21], and Liang et al. [22].

The experimental data and the fitting curves (Figure 9) indicate P_{CH} is not constant. P_{CH} increases when U_D grows.

Figure 10 is a comparative diagram showing the experimental data, the fitted curve, and the data of Touya et al. [34] and Sun [42], when $P_H = 0\,$MPa and the distance d between the discharge electrode and pressure sensor is 1 m. The experimental data and fitted curve are very different from the data of Touya and Sun Bing, but their trends are

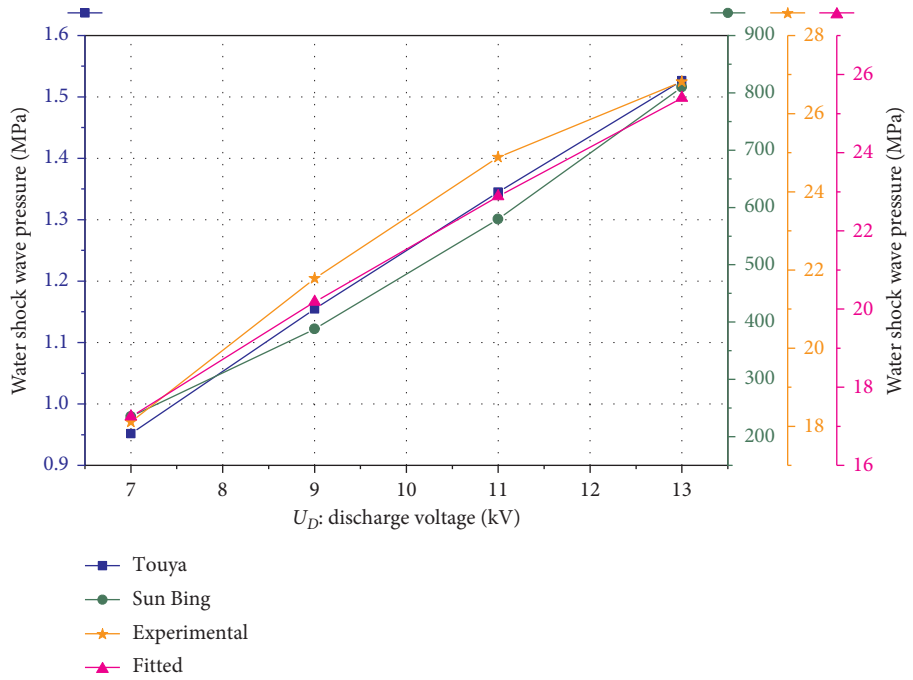

FIGURE 10: Comparative diagram showing the experimental U_D versus the water shock peak pressure with the fitted curve and the data of Touya and Sun Bing, using P_H of 0 MPa and d of 1 m.

similar. The differences are explained principally by the settings of Touya's experiment, in which the distance of the electrode gap l is 10 mm, the curvature radius r is 15 mm, $\alpha = 0.35$, and $k = 9000/d$ (d being the distance between the discharge electrode and pressure sensor). The equation of the maximum pressure P_T obtained by Touya is

$$P_T = \frac{9000}{d}(Q_B)^{0.35}, \tag{8}$$

where P_T is in bar, Q_B is in kJ, and d is in mm.

The pulsed discharge experiment of Touya was conducted in an open environment. One of the water boundaries was not restricted. This generates an energy loss during plasma expansion and impact on the free water surface, and the larger the distance d, the more prevalent is the drop in maximum pressure attributed to the loss. In this paper, the pulsed discharge experiments were carried out in an airtight pipeline which was fully filled with water, and $d = 1$ m (Touya's d values were 345–555 mm). The different discharge environments produce large deviations in Touya's calculations relative to our experimental values. The Touya's empirical equation is no longer applicable for water with all restricted boundaries (have no free surface), such as oil and gas wells filled with water.

The pulsed discharge experiments of Sun Bing were carried out with rod-rod electrodes in an airtight pipeline (5 m in length and 300 mm in diameter) filled with water (310 μS/cm). The empirical formula of peak pressure P_S by Sun Bing is

$$P_S = 2590 Q_D \cdot e^{-0.4836\times10^{-3}d}, \tag{9}$$

where P_S is in bar, Q_D is in kJ, and d is in mm.

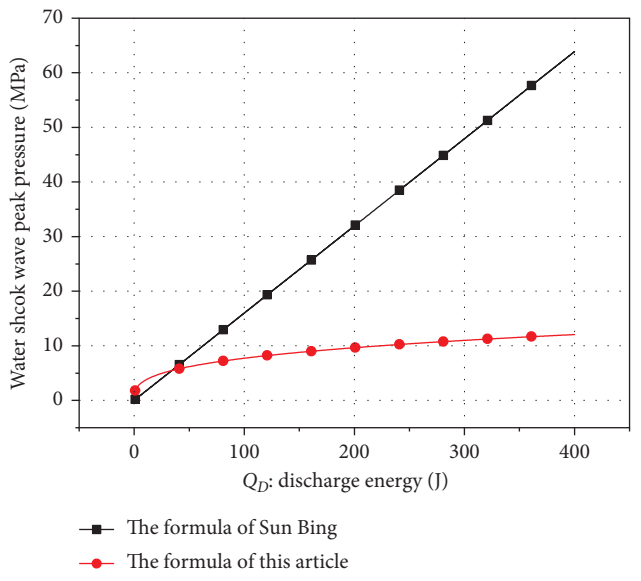

FIGURE 11: Comparison diagram showing the discharge energy (Q_D) versus water shock peak pressure using Sun Bing's formula and ours.

The maximum discharge energy of Sun Bing's experiment was 22.5 J ($C = 50$ nf and $U_D = 30$ kV). However, the minimum discharge energy of our experiments is > 1 kJ ($Q_D \approx 1.5$–5 kJ). Furthermore, the peak pressure P_S shows a linear correlation with the energy value Q_D when the distance d is constant.

Figure 11 shows that the deviation in the calculation results of the two formulas is small when $Q_D < 50$ J. However, if $Q_D > 50$ J, the deviation is more pronounced. The main

reason was the difference of discharge parameters between this two experiments (our experiment: $C = 60\,\mu$F and $U_D = 7$–13 kV. Sun Bing's experiment: $C = 50$ nF and $U_D = 22$–30 kV). Sun Bing's fitting formula was based on those experimental data which were obtained from high voltage ($U_D > 20$ kV) and small energy ($Q < 22.5$ J) discharge experiments. This led the efficiency of transforming the electrical energy into mechanical energy to be far higher than that of our experiment. For HVPD with larger energy (e.g., 1.5 kJ), the theoretical discharge voltage of Sun Bing was 200 kV (only 7 kV in our experiment). The calculations used Sun Bing's fitting formula (formula (9)), where the intensity of WSW was about 240 MPa and the energy conversion efficiency was about 180% (suppose the WSW width was $2\,\mu$s). Therefore, the empirical formula for peak pressure calculation by Sun Bing does not apply for a pulsed discharge process with larger Q_D.

5. Discussion

The relationship between the WSW properties (P_M, D_W, and η) and U_D and P_H was studied by experimentation. Results show that an increase of U_D can enhance the WSW properties (P_M, D_W, and η), but the processes of increasing P_H on the WSW properties (P_M, D_W, and η) are more complicated. The results obtained in this paper after fitting the experimental data are compared with that of other studies, and we explained discrepancies with the other published data. Through this study, we understood the basic method of controlling P_M and D_W. As a result, we can specifically modify the U_D and P_H values and then adjust the WSW properties (P_M and D_W) during the process of deep well fracturing.

In the process of HVPD, Jones found that the conductivity of water almost had no effect on the discharge process [28]. This is mainly because the discharge voltage of Jones' experiment was relatively higher ($U_D > 50$ kV), which caused the discharge breakdown process to be in nanoseconds. Thus, the influence of the conductivity on breakdown time delay was negligible basically. But when the discharge voltage was lower ($U_D < 5$ kV), the higher conductivity of water would lead to the shorter breakdown time delay [7, 30]. For the intensity of WSWs, Zhu et al. found that when $U_D = 4$ kV, with the conductivity increasing from 0 mS/cm to 120 mS/cm, P_M declined rapidly from 3.5 MPa to 0.62 MPa [29]. While Zhuang Jiasheng found that when $U_D = 7$ kV (HVPD was carried out in a pipe which had a parabolic reflector), with the conductivity increasing from 0.0177 mS/cm to 109.7 mS/cm, P_M increased from 20 MPa to 100 MPa [47]. Thus, under low discharge voltage, the influence of conductivity was huge and uncertain on intensity of WSWs. This means that a better fracturing effect of oil and gas wells can be achieved when using a fracturing fluid with suitable conductivity. So, the influence rules of conductivity on the intensity of WSWs need to be further studied.

Large capacity pulse capacitors were adopted in our experiment to store the electric energy. The capacitance value cannot be modified. If it was adjustable, we would need multiple parallel capacitors of small capacitance. However, this would bring the discharge process of each capacitor out of sync, release the pulse energy separately, and reduce the intensity of the first pulse shock wave [27].

The rise time of WSW obtained in this paper is significantly larger relative to other studies, and the P_H influence on the η value is unclear. This needs further research and analysis in the future.

6. Conclusions

When P_H is constant, T_B and R_L decreased, and I_P and P_P all increased. Furthermore, the WSW properties (P_M, D_W, and η) augmented with increasing U_D. A larger U_D always strengthened the effect of HVPD and the WSW properties.

Moreover, when U_D is constant, T_B and R_L increased and I_P and P_P all decreased with increasing P_H. The P_H augmentation demonstrated its "inhibiting" effect on the HVPD process. However, increasing P_H will partially reduce the attenuation coefficient of WSW and enhance the transfer of WSW. This demonstrates the "enhancing" effect on P_M and D_W. Thus, when U_D is constant, P_M and D_W first grow and then diminish with increasing P_H. This is caused by the inhibiting and the enhancing effects. Moreover, the η value of HVPD in pressurized liquid water is slightly smaller to that in stress-free water, but the change of η has no regularity.

The experimental data fitting enabled a partial application of the empirical formula which would provide a basis for theoretical calculation to further improve the permeability using pulsed discharge hydraulic fracturing.

Conflicts of Interest

The authors declare that they have no conflicts of interest.

Acknowledgments

Financial support for this work was provided in 2014 by the Coal-Based Key Tackling Item located in Shanxi Province (no. MQ2014-05). The authors would also like to thank the Institute of Coal Mining Technology for donating the experimental equipment and giving technical support.

References

[1] F. Zhou, Z. Chen, and S. Rahman, "Effect of hydraulic fracture extension into sandstone on coalbed methane production," *Journal of Natural Gas Science and Engineering*, vol. 22, pp. 459–467, 2015.

[2] Z. Zhou, H. Abass, X. Li, and T. Teklu, "Experimental investigation of the effect of imbibition on shale permeability during hydraulic fracturing," *Journal of Natural Gas Science and Engineering*, vol. 29, pp. 413–430, 2016.

[3] J. Han, Z. Yang, X. Li, and Y. Lu, "Present situation and pespectives of CBM of our country," *Journal of Chongqing University of Science and Technology*, vol. 14, no. 3, pp. 53–55, 2012.

[4] J. Zhang and S. Yin, "Some technologies of rock mechanics applications and hydraulic fracturing in shale oil, shale gas

and coalbed methane," *Journal of China Coal Society*, vol. 39, no. 8, pp. 1691–1699, 2014.

[5] Z. Feng, *The Theory and its Application on Gas Drainage in Low Permeability Coal Seam*, Ph.D. thesis, Taiyuan University of Technology, Shanxi, China, 2005.

[6] Y. Qin, A. Qiu, and Y. Zhang, "Experiment and discovery on permeability improved technology of coal reservoir based on repeated strong pulse waves of high energy accumulation," *Coal Science and Technology*, vol. 42, no. 6, pp. 1–8, 2014.

[7] L. Zhu, Z. He, P. Li et al., "The research on the pulsed arc electrohydraulic discharge and its application in treatment of the ballast water," *Journal of Electrostatics*, vol. 71, no. 4, pp. 728–733, 2013.

[8] A. I. Maksimov, I. K. Naumova, and A. V. Khlyustova, "Sterilization of solutions by underwater electric discharges," *High Energy Chemistry*, vol. 46, no. 3, pp. 212–215, 2012.

[9] P. Sunka, "Pulse electrical discharges in water and their application," *Physics of Plasma*, vol. 8, no. 5, pp. 2587–2594, 2001.

[10] H. Zhou, Y. Zhang, H. Li et al., "Generation of electrohydraulic shock waves by plasma-ignited energetic materials: III. Shock wave characteristics with three discharge loads," *IEEE Transactions on Plasma Science*, vol. 43, no. 12, pp. 4017–4023, 2015.

[11] S. H. Cho and K. Kaneko, "Influence of the applied pressure waveform on the dynamic fracture processes in rock," *International Journal of Rock Mechanics & Mining Sciences*, vol. 41, no. 5, pp. 771–784, 2004.

[12] H. Li, Y. Qin, Y. Zhang, Q. Shi, and X. Zhou, "Experimental study on the effect of strong repetitive pulse shockwave on the pore structure of fat coal," *Journal of China Coal Society*, vol. 40, no. 4, pp. 915–921, 2015.

[13] X. Zhou, Y. Qin, H. Li, Y. Zhang, A. Qiu, and Q. Shi, "Formation and development of coal micro-fractures under stress wave induced by electrical impulses," *Coal Science and Technology*, vol. 43, no. 2, pp. 127–130, 2015.

[14] K. Mare, D. Miroslaw, P. Janusz et al., "Characterisation of pulsed discharge in water," *Journal of Applied Physics*, vol. 64, no. 1, p. 10801, 2013.

[15] D. Oshita, S. Hosseini, Y. Miyamoto, K. Mawatari, and H. Akiyama, "Study of underwater shock waves and cavitation bubbles generated by pulsed electric discharges," *IEEE Transactions on Dielectrics and Electrical Insulation*, vol. 20, no. 4, pp. 1273–1278, 2013.

[16] Y. Sun, I. V. Timoshkin, M. J. Given et al., "Impulsive discharges in water: acoustic and hydrodynamic parameters," *IEEE Transactions on Plasma Science*, vol. 44, no. 10, pp. 2156–2166, 2016.

[17] A. Claverie, J. Deroy, M. Boustie et al., "Experimental characterization of plasma formation and shockwave propagation induced by high power pulsed underwater electrical discharge," *Review of Scientific Instruments*, vol. 85, no. 6, p. 063701, 2014.

[18] S. Lee, K. Chung, and Y. S. Hwang, "Correlation of the peak pressure generated by an underwater spark discharge with energy absorption in a spark channel," *Journal of the Korean Physical Society*, vol. 66, no. 12, pp. 1845–1851, 2015.

[19] P. Zhao and S. Roy, "A modified resistance equation for modeling underwater spark discharge with salinity and high pressure conditions," *Journal of Applied Physics*, vol. 115, no. 17, p. 173301, 2014.

[20] W. Jia, A. C. Qiu, F. Sun, and J. Guo, "Effects of pressure under the several hundred nanosecond pulse on the breakdown characteristics of the water switch," *High Voltage Engineering Science and Technology*, vol. 32, no. 1, pp. 50–52, 2006.

[21] Z. Zhang, J. Yang, J. Zhang, J. Liu, J. Pu, and Z. Liu, "Investigation of high electrical breakdown for pressurized water dielectric with microsecond charging," *High Power Laser and Particle Beams*, vol. 17, no. 5, pp. 761–764, 2005.

[22] C. Liang, L. Zhang, and X. Li, "Research on the pulsed breakdown of the pressured deionized water," *High Power Laser and Particle Beams*, vol. 16, no. 6, pp. 787–790, 2004.

[23] L. Xin-Pei, L. Ming-Hai, J. Zhong-He, and P. Yuan, "Effect of ambient pressure on bubble characteristics," *Chinese Physics Letters*, vol. 19, no. 5, pp. 704–706, 2002.

[24] J. A. Cook, A. M. Gleeson, R. M. Roberts, and R. L. Rogers, "A spark-generated bubble model with semi-empirical mass transport," *Journal of the Acoustical Society of America*, vol. 101, no. 4, pp. 1908–1920, 1997.

[25] X. Lu, Y. Pan, K. Liu, M. Liu, and H. Zhang, "Spark model of pulsed discharge in water," *Journal of Applied Physics*, vol. 91, no. 1, pp. 24–31, 2002.

[26] K. Chung, S. Lee, Y. S. Hwang, and C. Y. Kim, "Modeling of pulsed spark discharge in water and its application to well cleaning," *Current Applied Physics*, vol. 15, no. 9, pp. 977–986, 2015.

[27] Z. Qin, G. Zuo, Y. Wang, H. Wu, G. Sun, and Y. Sun, *High Voltage Pulse Discharge and its Applications*, Beijing Industrial University Press, Beijing, China, 2000.

[28] H. M. Jones and E. E. Kunhardt, "Pulsed dielectric breakdown of pressurized water and salt solutions," *Journal of Applied Physics*, vol. 77, no. 2, pp. 795–805, 1995.

[29] L. Zhu, Z. He, Z. Gao, F. Tan, X. Yue, and J. Chang, "Research on the influence of conductivity to pulsed arc electrohydraulic discharge in water," *Journal of Electrostatics*, vol. 72, no. 1, pp. 53–58, 2014.

[30] M. Jin and Y. Sun, "The electrical characteristics of underwater pulsed discharge under different experiment parameter," *High Voltage Engineering*, vol. 30, no. 7, pp. 46–49, 2004.

[31] V. Ushakov, V. F. Klimkin, and S. M. Korobeynikov, *Impulse Breakdown of Liquids*, Springer, Berlin, Germany, 2007.

[32] P. Barocha, V. Anita, N. Saito, and O. Takaia, "Bipolar pulsed electrical discharge for decomposition of organic compounds in water," *Journal of Electrostatics*, vol. 66, no. 5-6, pp. 294–299, 2008.

[33] X. Lu, Y. Pan, and H. Zhang, "The electrical and acoustical characteristics of pulsed discharge in water," *Chinese Physical Society*, vol. 51, no. 7, pp. 1549–1553, 2002.

[34] G. Touya, T. Reess, L. Pécastaing, and P. Domens, "Development of subsonic electrical discharges in water and measurements of the associated pressure waves," *Journal of Physics D: Applied Physics*, vol. 39, no. 24, pp. 5236–5244, 2006.

[35] J. Ning, C. Wang, and T. Ma, *Explosion and Shock Dynamics*, National Defence Industry Press, Beijing, China, 2010.

[36] I. Vitkovitsky, *High Power Switches*, Van Nostrand Reinhold Company, New York, NY, USA, 1978.

[37] J. P. VanDevender, "The resistive phase of a high-voltage water spark," *Journal of Applied Physics*, vol. 49, no. 5, pp. 2616–2620, 1978.

[38] K. C. Kao, "Breakdown of dielectric liquids," in *Proceedings of the Conference Report AIEE Winter Meeting*, pp. 60–84, New York, NY, USA, February 1960.

[39] S. Korobeinikov, *Bubble Model of Ignition of the Impulse Electric Discharge in Liquids*, Tomsk, Russia, 1998.

[40] E. Yanshin, S. Korobeynikov, and I. Ovchinnikov, "Physical processes limiting the pulse energy release in liquid dielectrics," in *Proceedings of the 10th IEEE International Pulse Conference*, Albuquerque, NM, USA, July 1995.

[41] J. Mirze, C. Smith, and J. Calderwood, "Bubbles, pressure and pre-breakdown in insulating liquid," in *Proceedings of the 4th International Conference on Conduction and Breakdown in Dielectric Liquids*, Dubin, Poland, September 1972.

[42] B. Sun, *Discharge Plasma in Liquid and its Applications*, Science Press, Beijing, China, 2013.

[43] A. Saul and W. Wagner, "A fundamental equation for water covering the range from the melting line to 1273 K at pressures up to 25000 MPa," *Journal of Physical and Chemical Reference Data*, vol. 18, no. 4, pp. 1537–1564, 1989.

[44] O. Maurel, T. Reess, M. Matallah et al., "Electrohydraulic shock wave generation as a means to increase intrinsic permeability of mortar," *Cement and Concrete Research*, vol. 40, no. 12, pp. 1631–1638, 2010.

[45] W. Chen, O. Maurel, T. Reess et al., "Experimental study on an alternative oil stimulation technique for tight gas reservoirs based on dynamic shock waves generated by Pulsed Arc Electrohydraulic Discharges," *Journal of Petroleum Science and Engineering*, vol. 88-89, pp. 67–74, 2012.

[46] Z. Lu, "Simulation research on relation between underwater explosive parameters and water pressure under a typical charge," *Torpedo Technology*, vol. 15, no. 1, pp. 45–47, 2007.

[47] J. Zhuang, *Development of an Electro-Hydraulic Liquid Shock Tube*, M.S. thesis, National Cheng Kung University, Taiwan, China, 2005.